Epitaxial pulsed laser crystallization of amorphous germanium on GaAs

P. V. Santos[a] and A. Trampert
Paul-Drude Institut, Hausvogteiplatz 5–7, 10117 Berlin, Germany

F. Dondeo and D. Comedi
Instituto de Física Gleb Wataghin, UNICAMP, Campinas 13083-970, São Paulo, Brazil

H. J. Zhu and K. H. Ploog
Paul-Drude-Institut, Hausvogteiplatz 5–7, 10117 Berlin, Germany

A. R. Zanatta
Instituto de Física de São Carlos, USP, São Carlos 13560-250, São Paulo, Brazil

I. Chambouleyron
Instituto de Física Gleb Wataghin, UNICAMP, Campinas 13083-970, São Paulo, Brazil

(Received 20 December 2000; accepted for publication 10 June 2001)

We have investigated the crystallization of amorphous germanium films on GaAs crystals using nanosecond laser pulses. The structure and composition of the crystallized layers is dominated by nonequilibrium effects induced by the fast cooling process following laser irradiation. Perfect epitaxial films are obtained for fluencies that completely melt the Ge film, but not the substrate. For higher fluencies, partial melting of the substrate leads to the formation of a $(GaAs)_{1-x}Ge_{2x}$ epitaxial alloy with a graded composition profile at the interface with the substrate. Since Ge and GaAs are thermodynamically immiscible in the solid phase, the formation of the alloy is attributed to the suppression of phase separation during the fast cooling process. Lower laser fluencies lead to polycrystalline layers with a patterned surface structure. The latter is attributed to the freeze-in of instabilities in the melt during the fast solidification process. © *2001 American Institute of Physics.* [DOI: 10.1063/1.1390312]

I. INTRODUCTION

Pulsed laser crystallization[1] (LC) of amorphous films proceeds through the heating (and eventually melting) of the amorphous layer induced by the absorption of a short laser pulse and the subsequent solidification in the crystalline phase. In its essence, the solidification process resembles liquid phase epitaxy (LPE). Contrary to conventional LPE, LC allows for a fast melting of the amorphous film through absorption of the laser pulse and for very high cooling rates. The latter has been explored in investigations of nonequilibrium phenomena during solidification. As far as the substrate is concerned, LC is essentially a low temperature process since only its region in contact with the amorphous film is exposed to high temperatures, and this for a very short time. This feature has turned LC into a standard technique for the fabrication of large area polycrystalline films of electronic quality on low-cost substrates.

Previous investigations of the LC process have mainly addressed the homoepitaxial crystallization of an amorphous film on a crystalline substrate of the same material (e.g., amorphized silicon on silicon[2]) or the crystallization of the amorphous film on a dissimilar substrate (e.g., silicon on glass[3]). The epitaxial laser crystallization of amorphous layers on a crystalline substrate has also been studied: examples are the crystallization of SiGe[4–6] and of SiGeC layers[7] on silicon substrates.

An interesting question associated with laser crystallization is how the structural properties of the irradiated layer and its interface with the substrate are affected by the fast melting and cooling times induced by laser irradiation. In this contribution, we address these questions by investigating the heteroepitaxial laser crystallization of an amorphous germanium (*a*-Ge) film on (100)-oriented crystalline GaAs substrates. This system represents an ideal one for studies of nonequilibrium effects on epitaxial crystal growth induced by fast cooling rates since crystalline Ge and GaAs are almost ideally lattice matched (lattice constant mismatch less the 0.1%) and have similar thermal expansion coefficients. In addition, Ge and GaAs are thermodynamically immiscible in the solid phase,[8,9] so that the Ge/GaAs interfaces are expected to remain abrupt after crystallization. By studying material intermixing and interface broadening induced by the laser pulses one can, therefore, obtain information about nonequilibrium effects on phase separation. In addition, the epitaxial growth of Ge on GaAs provides the GaAs technology with a low band gap material, which may be important for applications requiring monolithic infrared detectors for energies below 1.4 eV.

The investigations reported here were performed using Raman scattering and transmission electron microscopy (TEM). We demonstrate that the nanosecond melting and cooling of the Ge layers do not prevent crystallization in the form of high-quality dislocation-free epitaxial films with sharp interface with the substrate. The best epilayers are obtained for laser fluencies sufficiently high to melt the Ge

[a]Author to whom correspondence should be addressed; electronic mail: santos@pdi-berlin.de

film, but not the substrate. Outside this fluency regime, nonequilibrium phenomena dominate the crystallization process. Higher fluencies melt not only the a-Ge film but also the substrate: the fast cooling rates induce, in this case, the formation of a homogeneous epitaxial $(GaAs)_{1-x}Ge_{2x}$ layer with a composition close to that in the melt. The interface has a graded composition profile ranging between that of the substrate and that of the film. Since Ge and GaAs are thermodynamically immiscible in the solid phase, the formation of this graded composition range without phase separation yields direct evidence for the nonequilibrium conditions present during the rapid cooling down of the molten film. Lower laser fluency leads to crystallized layers with a periodically patterned surface. This structure is assigned to the excitations of capillary waves in the melt,[10] which, under appropriate conditions, may trigger the solidification process and freeze-in as a periodic surface undulation during the fast cooling process.

II. EXPERIMENT

The samples used in these studies consist of 100-nm-thick Ge films deposited on (100)-oriented GaAs using the ion-beam-assisted sputtering deposition system described in detail in Ref. 11. The target of 99.999% undoped germanium was bombarded by a beam of Kr^+ ions produced by an ion gun (beam energy of 1000 eV), and the sputtered Ge atoms were deposited on the surface of the GaAs wafers kept at 210 °C. Prior to Ge deposition, the GaAs surfaces were heated to 350 °C and bombarded by hydrogen ions produced by a second ion gun (beam energy of 30 eV) for 60 s. *In situ* monitoring using x-ray photoelectron spectroscopy showed that this procedure efficiently removes contaminants and the native oxide present at the surface.

The crystallization experiments were performed using single pulses from a frequency-doubled Nd:YAG laser ($\lambda_L = 532$ nm). The width of 7 ns of the Nd:YAG pulses is shorter than those of over 20 ns of conventional excimer lasers. The ns melting and cooling time scales employed here are substantially shorter than in previous investigations.[4,12] The laser beam profile was homogenized using a vacuum spatial filter, leading to a Gaussian- like intensity profile with a diameter $\phi_0 = 4$ mm on the sample surface. The integrated intensity of the laser pulses was adjusted using an attenuator consisting of a half wave plate and a polarizer. The pulse energy was measured for each pulse by deviating a portion of the laser beam to a detector. From the integrated intensity and from the diameter of the laser spot we determined the average fluency E_p and its radial distribution over the laser spot, as illustrated in Fig. 1 for a laser pulse with energy of 80 mJ. The laser exposures were carried out in air and at room temperature. The crystallization dynamics was monitored *in situ* by measuring the transient reflection (TR) of a continuous wave diode laser ($\lambda_P = 675$ nm, incidence angle of 67.5°) during the irradiation with the Nd:YAG pulse.[13]

The structural properties of the crystallized samples were investigated using cross-sectional TEM and Raman spectroscopy. The Raman measurements were performed in the backscattering geometry using different excitation wavelengths λ_R in order to probe different film depths. The incident light propagating along $z||[001]$ was polarized along the $x||[100]$ direction and the scattered light was analyzed either along $x||[100]$ ($z(xx)z$ configuration) or along $y||[010]$ ($z(xy)z$ configuration). Note that only the $z(xy)z$ configuration is symmetry-allowed for deformation potential Raman scattering from longitudinal optical (LO) phonons.[14]

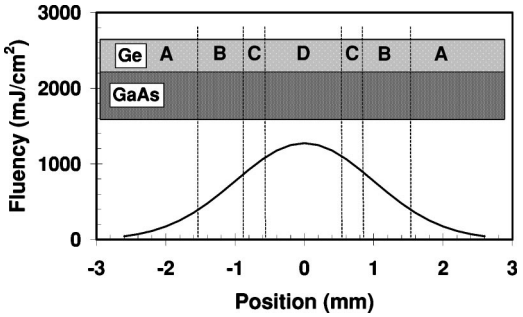

FIG. 1. Spatial distribution of laser fluency over the Ge surface (inset) for irradiation with a laser pulse with energy of 80 mJ and diameter of 4 mm. The approximate fluencies in regions *A*–*D* are: (*A*) less than 400 mJ/cm^2, (*B*) 400–900 mJ/cm^2, (*C*) 900–1100 mJ/cm^2, and (*D*) 1100–1300 mJ/cm^2.

III. RESULTS AND DISCUSSION

A. Crystallization dynamics

Typical TR reflection profiles obtained during the irradiation with the pulsed Nd:YAG beam are illustrated in Fig. 2. The duration of the laser pulse is indicated in the lower part of the diagram. For low pulse fluencies [Fig. 2(a)], the TR profiles have a pulse-like shape with width comparable to that of the crystallization pulse. Higher fluencies lead [cf. Figs. 2(c)–2(d)] to a plateau in the TR profile with a duration that depends on pulse fluency. The plateau is attributed to the formation on the film surface of a molten germanium layer

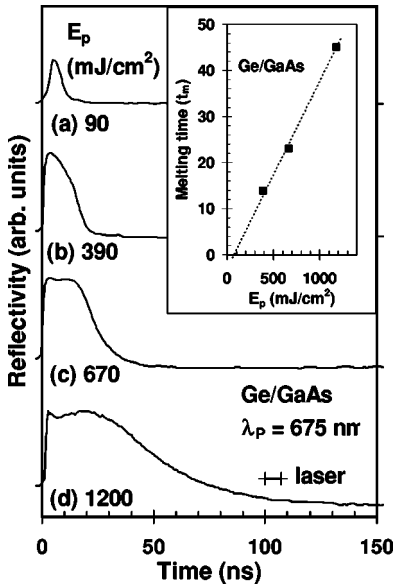

FIG. 2. Time-resolved reflection profiles obtained during the irradiation of Ge films on GaAs with laser pulses with average fluencies E_P of: (a) 90 mJ/cm^2, (b) 390 mJ/cm^2, (c) 670 mJ/cm^2, and (d) 1200 mJ/cm^2.

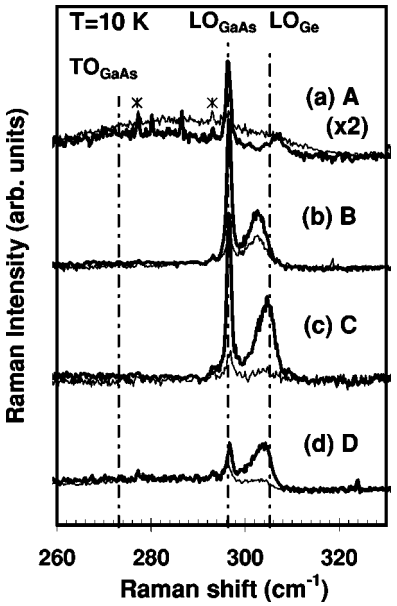

FIG. 3. Raman spectra measured at 10 K from Ge films on GaAs treated with laser pulses with energies in the ranges of intensity *A*–*D* indicated in Fig. 1. The thin and thick lines were recorded in the backscattering geometry with parallel $[z(xx)z$, thin lines] and crossed $[z(xy)z$, thick lines] polarizations of the incident and scattered radiation. The vertical dot-dashed lines indicate the position of LO and TO phonons in bulk GaAs and Ge (see Ref. 20). The 752.4 nm line from a Kr^+ laser was used for excitation. The peaks indicated by a * are plasma lines from the Kr^+ laser.

with metal-like reflectivity.[13,15–18] Note that the amplitude of the plateau, which depends on the difference between the reflectivity of liquid and solid germanium, does not depend on pulse fluency. The melting duration and the cooling time increase with laser fluency. From the dependence of the plateau duration on laser fluency (cf. inset) we estimate a fluency threshold for melting of the Ge film of $\sim$100 mJ/cm^2. Due to the higher heat conductivity of the GaAs substrates, this fluency is considerably larger than those necessary to crystallize amorphous germanium films deposited on glass substrates.[17]

B. Structural properties

The structure of the laser crystallized films depends strongly on laser fluency. From TEM and Raman measurements performed at different positions over the laser treated area, four structurally distinct regions (denoted as *A*–*D*) could be identified. The laser fluencies corresponding to these regions are indicated in Fig. 1. They were determined by performing several Raman measurements across a laser irradiation spot. Characteristic Raman spectra of the four regions are illustrated in Fig. 3. These spectra were recorded at 10 K using the 752.4 nm line from a Kr^+ laser for excitation. Under these conditions, the Raman probe depth in crystalline germanium (*c*-Ge) (of $\sim$100 nm) is comparable to the thickness of the Ge film, so that scattering from the GaAs substrate is also detected. The structural properties of each region will be described in detail below.

1. Region A

For low irradiation levels, the film structure corresponds to that of the as-deposited samples [region A in Fig. 4(a)], which is composed of an *a*-Ge matrix with small cone-like crystalline inclusions starting at the GaAs/Ge interface. Most of the inclusions form cones with the base at the interface and apices in the *a*-Ge matrix, some of them grow up to the film surface. The Raman spectra of Fig. 3(a) show that the c-Ge line from the inclusions (at $\omega_{LO}=306.3\pm0.2$ cm^{-1}) only appears in the $z(xy)z$ configuration, thus indicating that they are crystallographically oriented with the GaAs substrate. The spectrum in the $z(xx)z$ configuration is dominated by the broad Raman line from the *a*-Ge matrix centered at about 280 cm^{-1}.

2. Region B

For laser pulse fluencies between 400 and 900 mJ/cm^2 (region *B*), the films develop a structure consisting of two different regions [Fig. 4(b)]. Close to the Ge/GaAs interface the film crystallizes in the form of small grains with diameters between 10 and 20 nm [B_2 in Fig. 4(b)]. Some of these grains are misoriented with respect to the substrate. Above the layer of small grains, large grains develop with thicknesses of $\sim$80 nm and lateral dimensions (i.e., parallel to the surface) of $\sim$170 nm. The latter are much larger than the thickness of the original Ge film (region B_1). The large grains are well aligned with the substrate and contain a large density of twins and dislocations. The reduced phonon coherence induced by these defects is probably responsible for the relaxation of the polarization selection rules for Raman scattering, which is evidenced by the redshift of the phonon line and by the large scattering intensities for the forbidden $z(xx)z$ scattering configuration [Fig. 3(b)].

An interesting structural feature within fluency regime *B* is the pronounced surface roughening (amplitude of $\sim$15 nm) of the crystallized film. Surface roughening in laser crystallized silicon films was investigated by Fork and co-workers.[10] They proposed a model for the phenomenon based on the excitation of capillary waves by crystallization fronts propagating along the surface.[10] The capillary waves can be excited by the pressure exerted on the melt as the material contracts upon melting or when it expands upon solidification. In the case of laser crystallized silicon, the roughening is attributed to the latter process.[10] After nucleation takes place, two crystallization fronts propagating along opposite surface directions will eventually trap a capillary wave: ridges with high surface amplitude are then formed when the trapped wave freezes. The film structure with the boundaries of the large grains coinciding with the surface ridges, corresponds closely to that observed for the crystallized Ge films in Fig. 4(b).

A new feature in Fig. 4(b), which is not fully accounted for by the model described above, is the periodic nature of the surface roughening observed in some positions over the sample. The periodic undulation becomes evident in the TEM micrograph of a large surface area illustrated in Fig. 5. The undulation has a wavelength of $\sim$170 nm, which corresponds to the lateral dimensions of the large grains in region

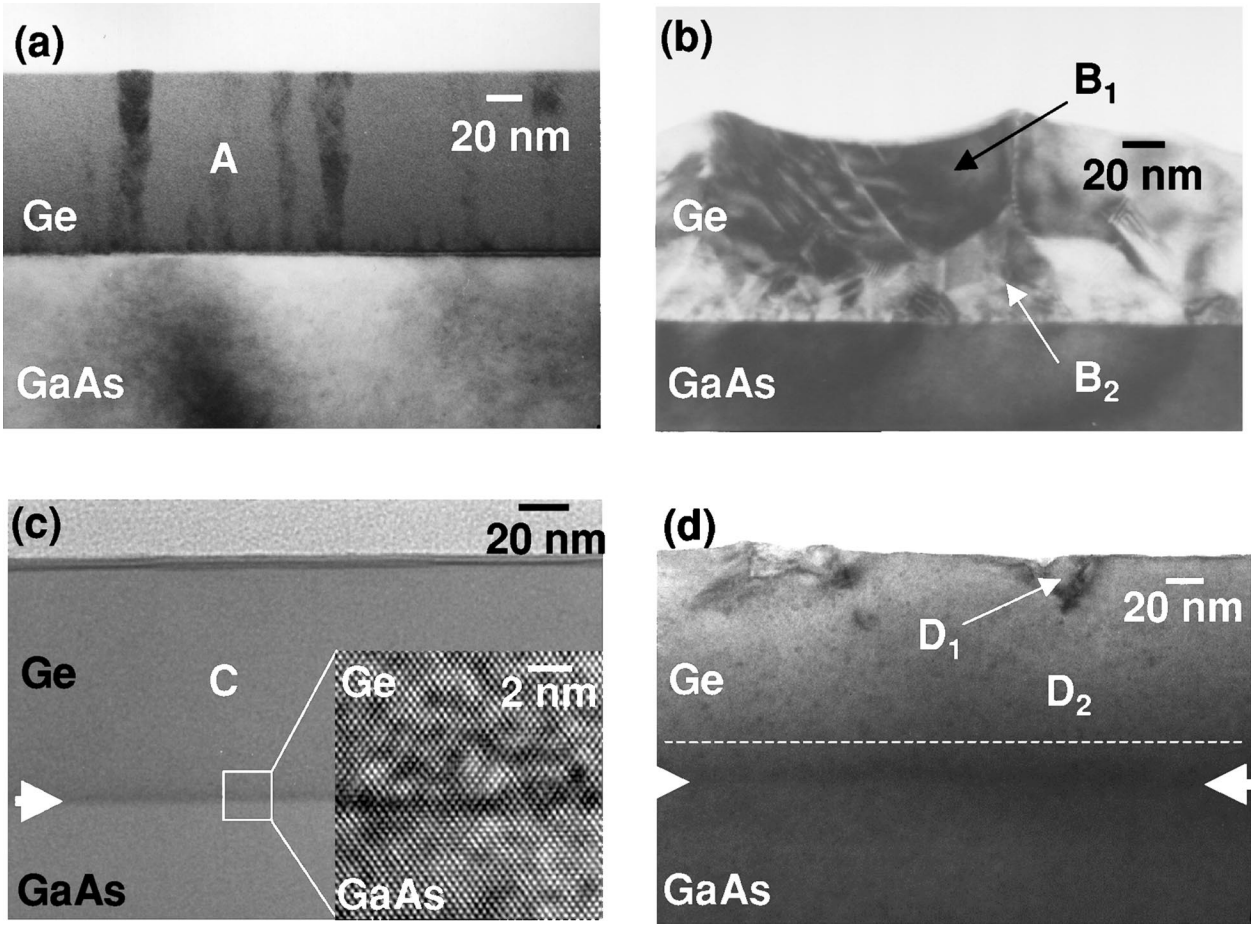

FIG. 4. Cross-section TEM micrographs of: (a) as-deposited Ge/GaAs films (region *A*) and after laser irradiation with fluencies in the regions (b) *B*, (c) *C*, and (d) *D* defined in Fig. 1. The dashed line in (d) marks the position of the Ge/GaAs interface before the laser treatment.

B_1. The periodic nature of the undulation indicates that the crystallization process itself is triggered by periodic fluctuations with a lateral coherence length far exceeding the film thickness. We propose that these fluctuations are induced by capillary waves generated *during melting* (and not *during solidification*, as suggested in Ref. 10). A possible scenario is described in the following: instabilities caused by volume changes during laser irradiation generate capillary waves in the melt with a wavelength of approximately twice the film thickness. Using the data for viscosity, surface tension, and density of liquid germanium from Ref. 19, we calculate an oscillation period and a decay time both in the range from 3 to 4 ns for capillary waves with a wavelength of 170 nm in a 100-nm-thick germanium melt. For sufficiently low fluencies, the melting time becomes comparable to the oscillation period and to the decay time of the capillary waves, as indicated in the inset of Fig. 2 (note that the melting times are plotted as a function of the average fluency E_P). The modulation in melt thickness induced by the capillary wave [of the order of 15% of the film thickness, cf. Fig. 4(b)] leads to a lateral temperature gradient with minima at the wave valleys, where the amount of stored thermal energy (proportional to the film thickness) is the lowest. These locations are then expected to freeze first, thus triggering a crystallization front propagating laterally. After that, a mechanism similar to that described in the last paragraph may then set in and lead to the morphology shown in Fig. 4(b).

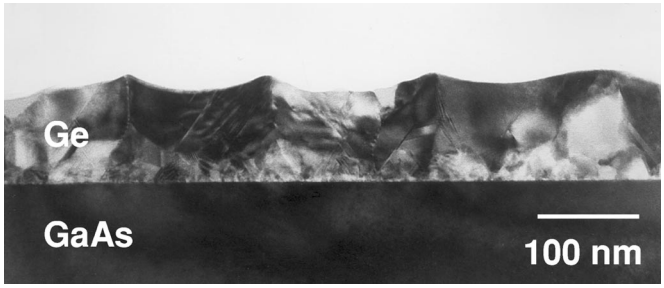

FIG. 5. Cross-section TEM micrograph showing surface undulations for fluencies in region B of Fig. 1.

3. Region C

Irradiation with laser fluencies in the range from 900 to 1100 mJ/cm^2 (region *C*) results in epitaxial Ge films with a sharp interface with the GaAs substrate, as shown in Fig. 4(c). The sample surface is perfectly flat in this case, thus indicating that the instabilities that give rise to the undulations in region *B* had already disappeared when the film crystallized. No structural defects like dislocations or stacking faults are detected in the epilayers, as it would be expected for perfect epitaxial growth of lattice matched materials.

The atomic configuration in the interface region is illustrated in the high resolution TEM (HRTEM) image displayed in the inset. The interface appears in the micrograph as a dark region with a width of ~2 monolayers. Due to the low contrast difference between GaAs and Ge in HRTEM, the dark region cannot be attributed to the intermixing of substrate and film materials at the interface. Though specific investigations have not been carried out to address its nature, we attribute the dark region to residual impurities (in the submonolayer range) present on the surface of the GaAs wafers prior to the Ge deposition, which remain trapped at the interface after the crystallization process. The low impurity concentration does not disturb the perfect atomic alignment across the interface after laser crystallization,[5] as illustrated in the high resolution images displayed in the inset. The Raman spectra [Fig. 3(c)] display a strong Ge-like LO line in the $z(xy)z$ configuration and almost no scattering in the $z(xx)z$ forbidden geometry, in agreement with the predictions for an epitaxial layer. We conclude, therefore, that the high temperatures and fast cooling rates present during laser crystallization do not prevent crystallization in the form of high-quality, dislocation-free epitaxial films with sharp interface with the substrate.

4. Region D

For pulse energies corresponding to regions *A*–*C* the Ge/GaAs interface remains abrupt and essentially undisturbed during the crystallization process. The laser fluency in these cases is sufficiently strong to melt the Ge layers but not the GaAs substrate, which has a 300 K higher melting point (the melting temperatures of Ge and GaAs are 1210.4 and 1513 K, respectively[20]). When the fluency exceeds 1100 mJ/cm^2 [region *D*, Fig. 4(d)], the original Ge/GaAs interface moves towards the substrate [by 25 nm in Fig. 4(d)], thus indicating that the latter also melts [the original position of the interface is indicated by the dashed line in Fig. 4(d)]. The interface also becomes significantly broader, thus evidencing considerable material intermixing. It is interesting to note that in the region from the interface up to ~30 nm from the surface [denoted as region D_2 in Fig. 4(d)], the Ge layer crystallizes epitaxially with structural properties similar to those found in region *C*. The epitaxial nature is also reflected in the large ratios between the Raman intensity in the $z(xy)z$ and the $z(xx)z$ scattering geometries [Fig. 3(d)]. Near the surface [region D_1], however, the TEM micrographs reveal the presence of inclusions in the crystalline Ge matrix. These inclusions have lattice constants and crystallographic orientation differing from that of the surrounding Ge matrix.

Dark field TEM analysis was applied to compare the interface sharpness in regions *C* and *D* in more detail. For that purpose, we exploit the fact that the (200) and the $(\bar{2}00)$ reflections are kinematically forbidden for the diamond Ge structure, but not for zinc blende GaAs structure. The cross-sectional samples were tilted out of the exact ⟨110⟩ zone axis position in order to produce strong diffraction by only the {200} atomic planes which are parallel to the interface. {200} dark field images of regions *C* and *D* are displayed in Figs. 6(a) and 6(b), respectively, together with intensity line scans perpendicular to the interface. The tilt angle was adjusted in an identical way for both image conditions; the thickness of the specimen regions is also comparable in both cases. As expected, the Ge epilayers and the GaAs substrate appear, respectively, dark and bright in both micrographs. The effective width of the Ge/GaAs interface in region *C*, of ~2.5 nm [cf. Fig. 6(a)], is determined by the instrumental resolution for this particular measurement conditions. In region *D* the interface width increases to 25 nm.

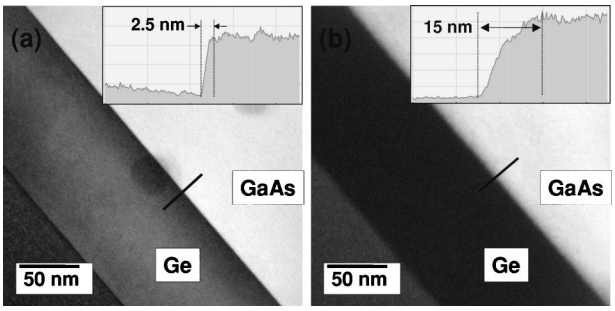

FIG. 6. Dark field TEM micrographs obtained from reflections from the {200} planes perpendicular to the Ge/GaAs interface for fluency regions (a) *C* and (b) *D* [cf. Fig. 1(b)]. The insets display intensity profiles of the [200] reflex across the interface recorded along the scan line indicated in the figure.

We attribute the interface broadening to the formation of an epitaxial $(GaAs)_{1-x}Ge_{2x}$ alloy with a wide range of compositions x through interdiffusion, when the material is melted by the laser pulse. As mentioned before, Ge and GaAs are thermodynamically immiscible in the solid phase.[8,9] The fact that the interface alloy forms without phase separation provides direct evidence for the nonequilibrium conditions prevailing during solidification.

C. Film composition

Information about the composition of the laser crystallized films and about the degree of intermixing with the substrate can be obtained from Raman spectroscopy. The Raman spectra of the crystallized layers (Fig. 3) display a strong Ge-like LO line in the $z(xy)z$ configuration. In the epilayers [Figs. 3(c) and 3(d)], there is almost no scattering in the $z(xx)z$ geometry, in agreement with the selection rules for deformation potential Raman scattering. The Raman lines for the epilayers, however, are redshifted, asymmetric, and considerably broader than for bulk Ge (linewidth <0.9 cm^{-1} at low temperatures).

The position and width of the Ge Raman line is expected to be sensitive to stress,[18] doping,[21,22] grain size,[18,23,24] and, in the case of $(GaAs)_{1-x}Ge_{2x}$, to the composition x.[25–27] In the present case, the grain sizes are large enough to have a negligible effect on phonon frequencies.[18] The presence of defects within the grains, however, may limit the phonon coherence length in a similar way as grain boundaries do, leading thus to a red-shift of the Raman line. In regions *C* and D_2, which correspond to epitaxial films, stress effects can also be discarded due to the good lattice match between GaAs and Ge.

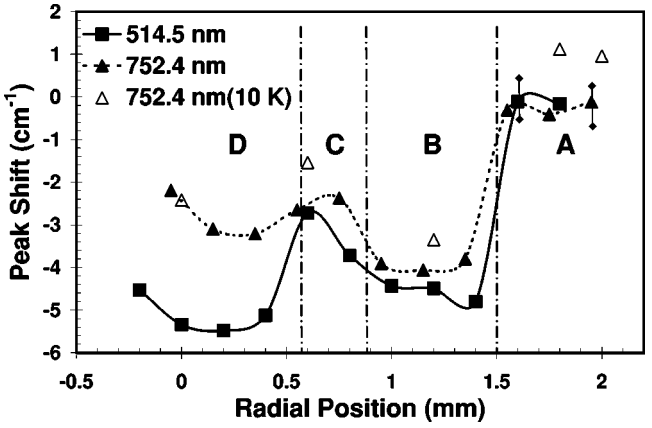

FIG. 7. Dependence of the energy of the Ge-like Raman line on position over the laser spot for laser crystallized Ge films on GaAs (the relationship between laser fluency and position is displayed in Fig. 1). The Raman shifts are relative to the position of the LO Raman line from crystalline germanium at room temperature. The Raman measurements were performed at room temperature using excitation wavelengths of 514.5 nm (square, probing depth $d_R = 8.5$ nm) and 752.4 nm (triangles, $d_R = 80$ nm). The triangles display results measured with the 752.4 nm line at 10 K.

The shape of the Raman spectrum is similar to those reported for Ge rich $(GaAs)_{1-x}Ge_{2x}$ alloys with x close to unity,[25–27] thus suggesting that the modifications in the Raman line are associated with the incorporation (and possibly doping) of Ga and/or As atoms from the substrate. According to Ref. 25, the incorporation of substrate species leads to a substantial broadening and to a redshift r_R of the Ge-like LO line (ω_{LO}). The latter can be expressed as: $r_R = -\partial\omega_{LO}/\partial(1-x) = 0.28\ cm^{-1}/\%$ of GaAs incorporation in Ge for $0.8 < x < 1$. In order to obtain information about the composition of the films, we will assume that the same mechanism applies for the laser crystallized layers. In this case, we estimate from the ω_{LO} positions in Fig. 3 effective (i.e., averaged over the film thickness) GaAs alloy fractions $x_{eff} = 5.5 \pm 1.5\%$ and $x_{eff} = 9 \pm 1.5\%$ for regions *C* and *D*, respectively.

Information about the composition profile in the growth direction can be extracted from Raman measurements with different excitation wavelengths (and, therefore, different probing depths). Figure 7 displays the frequency shift of the Ge-like LO Raman line (relative to the frequency of the Raman line for bulk Ge at room temperature), as a function of position from the center of the crystallization spot for a sample irradiated under the conditions described in Fig. 1, from which the fluency dependence on position can be extracted. The measurements were performed at room temperature using excitation wavelengths of $\lambda_L = 514.5$ nm (corresponding to a probing depth $d_R = 8.5$ nm) and 752.4 nm ($d_R = 80$ nm). Within the experimental resolution, the Raman shifts for the two excitation energies coincide for regions *A–C*, thus indicating a homogeneous film composition along the growth direction. The same applies for measurements performed at 10 K (triangles, the shift of $\sim 1\ cm^{-1}$ is due to the higher phonon frequencies at low temperatures). For region *D*, however, the material near the surface exhibits a considerably larger redshift, in qualitative agreement with the two-layer structure displayed in Fig. 4(d). The redshift is attributed to the inclusions observed in region D_1.

The effective alloy fractions x_{eff} determined above fall within the range of equilibrium compositions calculated for $(GaAs)_{1-x}Ge_{2x}$ alloys[9] of $x \sim 3\%$ and $x \sim 10\%$ at the Ge and GaAs melting points, respectively. These results suggest the following scenario for the crystallization process in fluency regions *C* and *D*. When the *a*-Ge films melt upon laser irradiation, the GaAs material in contact with the film partially dissolves into the melt. Since diffusion processes are very fast in the liquid state, the concentration of Ga and As species is expected to be relatively homogeneous in the melt and to achieve values comparable to the equilibrium ones at the melt temperature. Due to the dissolution process, the interface between the film and substrate remains relatively abrupt even when a large concentration of substrate species is incorporated into the melt [cf. Fig. 6(d)]. The melt cools down mainly through heat extraction across the interface with the substrate. The epitaxial regrowth starts from this interface. During the fast regrowth, a concentration of Ga and As species corresponding to the equilibrium concentration at the freezing temperature is frozen-in the solid. The fast cooling rates prevent subsequent phase separation in the solid phase, thus yielding a homogeneous $(GaAs)_{1-x}Ge_{2x}$ alloy with a composition x close to that present in the melt. High laser fluencies (as for region *D*) may lead to a high concentration of substrate species in the melt. The inclusions in region D_1 [cf. Fig. 4(d)] may arise from the precipitation of a Ga-rich phase when a large amount of substrate material dissolves in the melt and As atoms effuse from the sample. In fact, a high Ga concentration near the surface was reported for Ge/GaAs structures annealed using a cw laser.[4] Further experiments are underway to clarify this point.

IV. CONCLUSIONS

In conclusion, we have investigated the structure and composition of pulsed laser crystallized *a*-Ge films on GaAs and correlated these properties with the laser irradiation conditions. The film properties depend sensitively on the irradiation fluency, which controls the thickness of the molten Ge layer and the melt duration. Under appropriate conditions, laser crystallization can be employed to produce epitaxial layers with high structural quality on GaAs.

ACKNOWLEDGMENTS

The authors thank M. Ramsteiner and S. K. Zhang for discussions and for assistance with the Raman measurements, and J. Herfort for a careful reading of the manuscript. The investigations were partially supported by a DAAD (Germany)-CAPES (Brazil) International Cooperation Program.

[1] *Laser Annealing of Semiconductors*, edited by J. M. Poate and J. W. Mayer (Academic, New York, 1982).
[2] A. G. Cullis, H. C. Weber, N. G. Chew, J. M. Poate, and P. Baeri, Phys. Rev. Lett. **49**, 219 (1982).
[3] C. K. Celler, H. J. Leamy, D. E. Aspnes, C. J. Doherty, T. T. Sheng, and L. E. Trimble, in *Laser and Electron-Beam Solid Interactions and Materials Processing*, edited by J. K. Gibbons, L. D. Hess, and T. W. Sigmon (Elsevier, North Holland, Inc., Amsterdam, 1981), p. 435.

[4] J. E. Greene, K. C. Cadien, D. Lubben, G. A. Hawkins, G. Erikson, and J. R. Clarke, Appl. Phys. Lett. **39**, 232 (1981).
[5] J. R. Abelson, T. W. Sigmon, K. B. Kim, and K. H. Weiner, Appl. Phys. Lett. **52**, 230 (1988).
[6] S. Lombardo, P. M. Smith, J. J. Uttomark, D. P. Brunco, K. Kramer, and M. O. Thompson, Appl. Phys. Lett. **58**, 1768 (1991).
[7] E. Finkman, J. Boulmer, P. Boucaud, C. Guerj, D. Bouchier, K. Nugend, and S. Prawer, Appl. Surf. Sci. **106**, 171 (1996).
[8] K. E. Newman and J. D. Dow, Phys. Rev. B **27**, 7495 (1983).
[9] R. Osório, S. Froyen, and A. Zunger, Phys. Rev. B **43**, 14 055 (1991).
[10] D. K. Fork, G. B. Anderson, J. B. Boyce, R. I. Johnson, and P. Mei, Appl. Phys. Lett. **68**, 2138 (1996).
[11] D. Comedi, F. Dondeo, I. Chambouleyron, Z. L. Peng, and P. Mascher, J. Non-Cryst. Solids **266**, 713 (2000).
[12] K. M. Lui, K. P. Chik, and J. B. Xu, Appl. Phys. Lett. **70**, 865 (1997).
[13] G. Aichmayr, D. Toet, M. Mulato, P. V. Santos, A. Spangenberg, S. Christiansen, M. Albrecht, and H. P. Strunk, J. Appl. Phys. **85**, 4010 (1999).
[14] M. Cardona, in *Light Scattering in Solids II*, edited by M. Cardona and G. Güntherodt (Springer, Heidelberg, 1982), p. 19.
[15] *Semiconductors and Semimetals*, edited by R. F. Wood, C. W. White, and R. T. Young (Academic, New York, 1984), Vol. 23.
[16] *Laser and Electron Beam Processing of Materials*, edited by C. W. White and P. S. Piercy (Academic, New York, 1980).
[17] M. Mulato, D. Toet, G. Aichmayr, P. V. Santos, and I. Chambouleyron, Appl. Phys. Lett. **70**, 3570 (1997).
[18] M. Mulato, D. Toet, G. Aichmayr, P. V. Santos, and I. Chambouleyron, J. Appl. Phys. **82**, 5159 (1997).
[19] *Landolt-Börnstein Tables Vol. 17c*, edited by H. W. O. Madelung and M. Schulz (Springer, Heidelberg, 1984).
[20] *Landolt-Börnstein Tables Vol. 17a*, edited by O. Madelung (Springer, Heidelberg, 1982).
[21] F. Cerdeira and M. Cardona, Phys. Rev. B **5**, 1440 (1972).
[22] D. Olego and M. Cardona, Phys. Rev. B **23**, 6592 (1981).
[23] P. M. Fauchet and I. H. Campbell, Crit. Rev. Solid State Mater. Sci. **14**, S79 (1988).
[24] H. Richter, Z. P. Wand, and L. Ley, Solid State Commun. **39**, 625 (1981).
[25] S. A. Barnett, M. A. Ray, A. Lastras, B. Kramer, J. E. Greene, P. M. Raccah, and L. L. Abels, Electron. Lett. **18**, 891 (1982).
[26] K. A. Newman, J. D. Dow, B. A. Bunker, L. L. Abels, P. M. Raccah, S. Ugur, D. Z. Xue, and A. Kobayashi, Phys. Rev. B **39**, 657 (1989).
[27] B. Salazar-Hernández, M. A. Vidal, M. E. Constantino, and H. Navarro-Contreras, Solid State Commun. **109**, 295 (1999).